

Low-frequency hiss-like whistler-mode waves generated by nonlinear three-wave interactions outside the plasmasphere

Cite as: Phys. Plasmas **26**, 122901 (2019); <https://doi.org/10.1063/1.5115542>

Submitted: 19 June 2019 . Accepted: 04 November 2019 . Published Online: 03 December 2019

Zhonglei Gao , Zhengyang Zou, Pingbing Zuo , Yi Wang , Zhaoguo He, and Fengsi Wei



[View Online](#)



[Export Citation](#)



[CrossMark](#)

ARTICLES YOU MAY BE INTERESTED IN

Numerical simulations to study turbulent magnetic field amplification by nonlinear interaction of high-power laser and kinetic Alfvén waves in laboratory and astrophysical plasmas
Physics of Plasmas **26**, 122105 (2019); <https://doi.org/10.1063/1.5113933>

A three-dimensional model of spiral null pair to form ion-scale flux ropes in magnetic reconnection region observed by Cluster
Physics of Plasmas **26**, 112901 (2019); <https://doi.org/10.1063/1.5114620>

Spatio-temporal behavior of magnetohydrodynamic fluctuations with cross-helicity and background magnetic field
Physics of Plasmas **26**, 122301 (2019); <https://doi.org/10.1063/1.5129655>



The advertisement features a dark blue background with white snowflake icons. The text "AIP Conference Proceedings" is in white, and "FLASH WINTER SALE!" is in large red capital letters. A red banner at the bottom contains the text "50% OFF ALL PRINT PROCEEDINGS" and "ENTER CODE 50DEC19 AT CHECKOUT".

Low-frequency hiss-like whistler-mode waves generated by nonlinear three-wave interactions outside the plasmasphere

Cite as: Phys. Plasmas **26**, 122901 (2019); doi: [10.1063/1.5115542](https://doi.org/10.1063/1.5115542)

Submitted: 19 June 2019 · Accepted: 4 November 2019 ·

Published Online: 3 December 2019



View Online



Export Citation



CrossMark

Zhonglei Gao,^{1,2,a)} Zhengyang Zou,¹ Pingbing Zuo,¹ Yi Wang,¹ Zhaoguo He,³ and Fengsi Wei¹

AFFILIATIONS

¹Institute of Space Science and Applied Technology, Harbin Institute of Technology, Shenzhen 518055, China

²School of Physics and Electronic Sciences, Changsha University of Science and Technology, Changsha 410114, China

³School of Atmospheric Science, Sun Yat-sen University, Zhuhai 519082, China

^{a)}gaozhl@outlook.com

ABSTRACT

Whistler-mode waves play an important role in the inner magnetospheric particle dynamics. The direction and efficiency of energy transfer between waves and particles strongly depend on the wave frequency distribution characteristics. Recent observations have drawn attention to the low-frequency whistler-mode chorus waves below 0.1 times the equatorial gyrofrequency f_{ce} of electrons outside the plasmasphere. Here, on the basis of the analysis of the Van Allen Probes wave data, we describe a new type of low-frequency hiss-like whistler-mode wave around or below 0.1 f_{ce} . We show that two normal chorus wave bands split by the 0.5 f_{ce} gap can produce the low-frequency hiss-like whistler-mode waves through the nonlinear three-wave interaction.

Published under license by AIP Publishing. <https://doi.org/10.1063/1.5115542>

I. INTRODUCTION

Whistler-mode waves are one of the most important electromagnetic waves outside the plasmasphere.^{1–5} Abundant observations and simulations have demonstrated the energy transfer between magnetospheric particles and various whistler-mode waves,^{6–13} e.g., chorus and exohiss. The direction and efficiency of energy transfer between particles and waves strongly depend on the wave frequency distribution characteristics.^{14,15} It is important to understand how the whistler-mode waves in the different frequency ranges are generated.

Chorus waves normally occur in the frequency range of 0.1–0.8 f_{ce} , with a gap of around 0.5 f_{ce} .^{16,17} In the high-resolution frequency-time spectrograms, these waves usually appear as a series of quasimonochromatic elements (e.g., risers, faller, constant/oscillating tones, and hooks) or a structureless hiss-like broad band.^{18–21} The frequency distribution of the normal chorus has been successfully reproduced by the linear instability theory of hot electrons,^{22,23} and various nonlinear wave-particle theories have been proposed to explain the high-resolution wave structures.^{24–26} Slightly below 0.1 f_{ce} , there are exohiss waves in the dayside magnetosphere.^{14,27,28} Observation and simulation have demonstrated that the exohiss waves are the plasmaspheric hiss waves leaking through the plasmapause.^{14,29,30}

Recent observations^{15,31–33} have drawn attention to the low-frequency whistler-mode chorus waves below 0.1 f_{ce} . Statistical results

indicate that they prefer to occur near high AE and the minimum Dst during geomagnetic storms.³¹ Xiao *et al.*³² and Yu *et al.*³³ both attempted to explain the generation of low-frequency chorus in the framework of the linear instability theory. Xiao *et al.*³² attributed the efficient growth of low frequency waves to a high-energy tail of the hot electron population. Later, Yu *et al.*³³ found that the chorus wave growth below 0.1 f_{ce} could occur in the high density environment, analogous to the situation of whistler-mode hiss in the plasmasphere and plasmaspheric plume.^{34,35}

In this study, we describe a new type of low-frequency hiss-like whistler-mode waves around or below 0.1 f_{ce} . We show that these waves are generated by the nonlinear three-wave interactions between two normal chorus bands, essentially different from the previously reported waves^{15,31–33} produced by the wave-particle interactions. Note that, in recent years, various nonlinear wave-wave interactions have been invoked to explain the multibanded³⁶ or highly oblique^{37,38} chorus waves and the magnetosonic harmonic frequency-sweeping structures.³⁹

II. DATA AND METHODS

NASA launched the Van Allen Probes on 30 August 2012, aiming to discover the fundamental physics of the Van Allen radiation belts.⁴⁰ The helium, oxygen, proton, and electron mass spectrometer⁴¹

and the magnetic electron ion spectrometer⁴² of the energetic particle, composition, and thermal plasma suite⁴³ can measure the electron fluxes at energies of 1.5 eV–3.8 MeV. The electric and magnetic field instrument suite and integrated science suite⁴⁴ on the probes can provide the survey mode wave power spectral density (PSD), the continuous-burst mode waveform, and the background magnetic field. Each waveform sequence lasts ~6 s with a 35 kHz sampling rate. By applying a 1024-point fast Fourier transform on the waveforms, we can get the high-resolution wave spectral matrices. Then, we use the wave spectral matrices to calculate the magnetic polarization information of the waves through the singular value decomposition method.⁴⁵ The calculation is performed in the field-aligned coordinate system defined as follows: the Z-axis parallel to the background magnetic field, the X-axis along the cross product of the satellite spin axis and the Z axis, and the Y-axis completing the right-handed triad. The wave

normal angle is the angle between the wave vector and the Z-axis, and the wave azimuthal angle is defined as the angle between the X-axis and the projection of the wave vector in the X-Y plane. We model the ratio between electron gyrofrequencies at the equator and at the probe using the TS04 package.⁴⁶

III. OBSERVATIONS

The geospace environment on 13 November 2016 is shown in Fig. 1. There were some strong substorms (AE maximum of 1000 nT) but no storms (SYM-H > -30 nT). The upper hybrid frequency in the high frequency electric power spectra [Fig. 1(b)] indicates that Probe A was in the low density plasma trough during 18:00–23:10 UT. After 19:40 UT, Probe A observed the substorm-injected hot electrons [Fig. 1(d)] and the locally excited whistler-mode chorus waves around 0.5 f_{ce} [Fig. 1(c)]. Below the normal chorus, there was a low-frequency

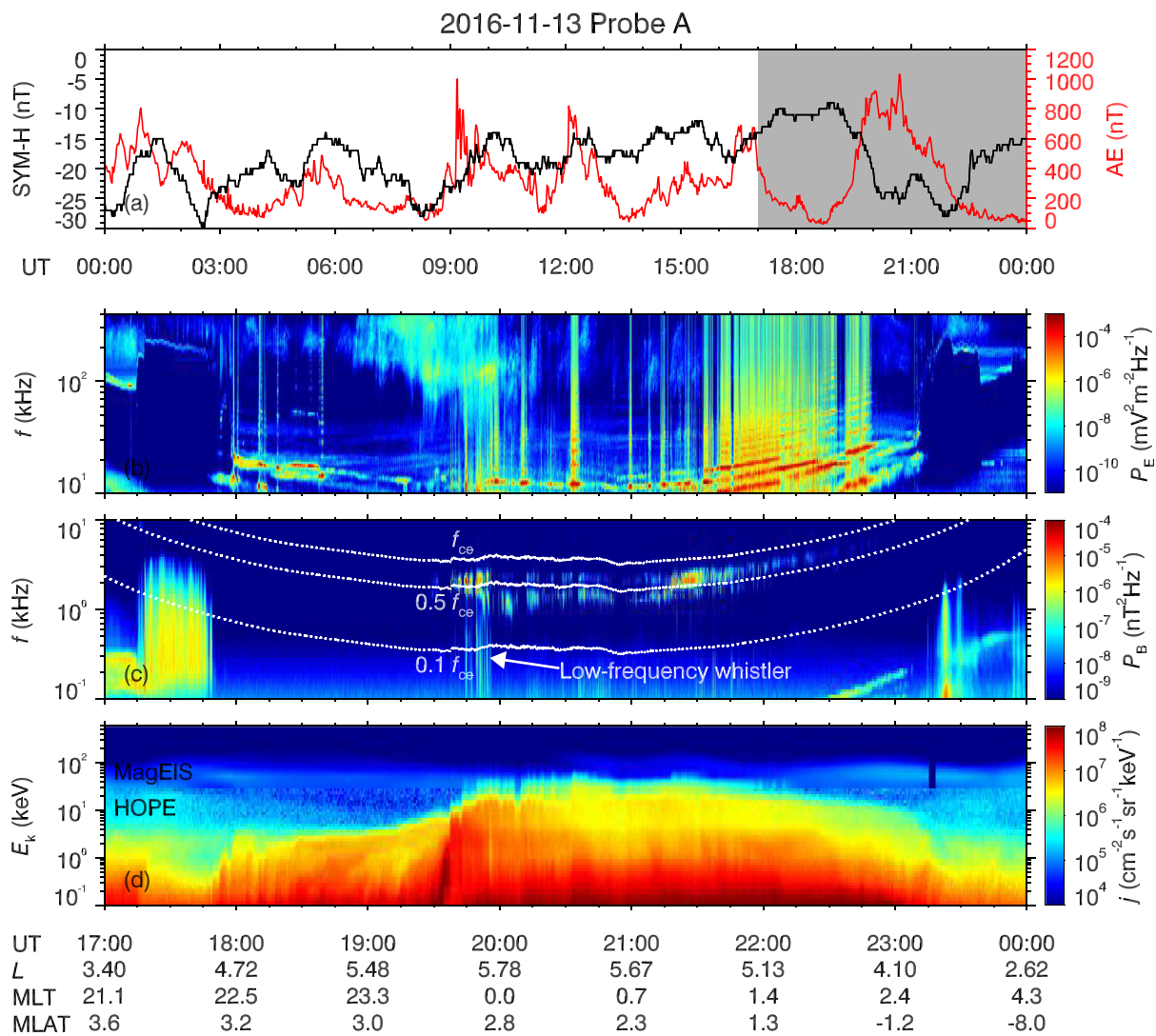


FIG. 1. Space environment overview on 13 November 2016: (a) geomagnetic activity indices AE and SYM-H; (b) high frequency electric power spectra P_E ; (c) low frequency magnetic power spectra P_B ; and (d) electron differential fluxes j . In Fig. 1(c), the dotted lines represent $0.1 f_{ce}$, $0.5 f_{ce}$, and f_{ce} , respectively.

whistler-mode band [pointed by an arrow in Fig. 1(c)]. The observed low-frequency band was unlikely to be the exohiss waves. In the nightside magnetosphere, the plasmaspheric hiss leaking from the high-latitude plasmapause would be strongly damped by hot electrons.

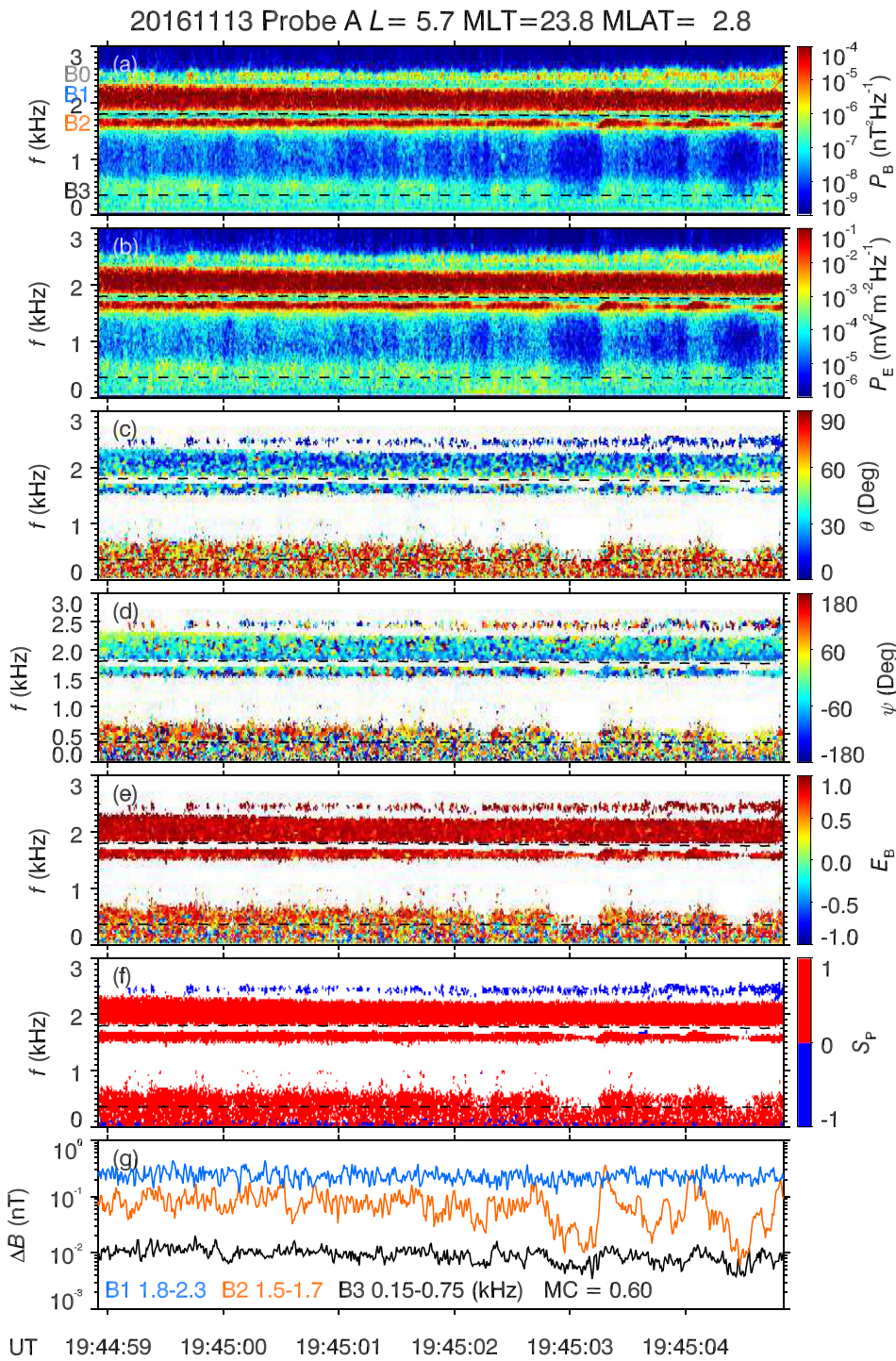


Figure 2 shows a selected burst-mode event of whistler waves observed around 19:45 UT ($L = 5.7$, $\text{MLT} = 23.8$, and $\text{MLAT} = 2.8$). In the electromagnetic power spectrograms [Figs. 2(a) and 2(b)], four whistler wave bands can be identified. For convenience, we number these bands 0, 1, 2, and 3 from the top to bottom according to their

FIG. 2. High-resolution observations of whistler waves: [(a) and (b)] electromagnetic power spectra P_B and P_E ; [(c) and (d)] normal angle θ and azimuthal angle ψ ; (e) wave ellipticity E_B ; (f) sign of the parallel component of the wave Poynting flux S_P (positive for northward and negative for southward); and (g) wave amplitudes ΔB of three wave bands. The dashed lines in each figure represent 0.1 and 0.5 f_{ce} . Four wave bands abbreviated to “B0, B1, B2, and B3” and the frequency ranges of our concerned three ones are labeled in Figs. 2(a) and 2(g). MC in Fig. 2(g) represents the multiple correlation coefficient of the amplitude’s logarithm of B3 on those of B1 and B2.

frequencies. Above $0.5 f_{ce}$, there were two bands: the southward-propagating narrow band 0 around the frequency of 2.5 kHz and the northward-propagating hiss-like band 1 in the frequency range of 1.8–2.3 kHz. Just below $0.5 f_{ce}$, the northward-propagating narrow band 2 occurred at a nearly constant frequency 1.7 kHz. The northward-propagating band 3 was the low-frequency hiss-like whistler mentioned in Fig. 1(c), with the lower frequency cutoff of ~ 150 Hz ($0.04 f_{ce}$). The normal chorus bands 0–3 were right-hand circularly polarized (ellipticities close to 1) and had quasiparallel normal angles (from $\sim 20^\circ$ to 30°) and largely fluctuating azimuthal angles (from -90° to 90°). In contrast, for the whistler band 3, the ellipticities decreased to ~ 0.5 , the normal angles increased to $\sim 60^\circ$, and the azimuthal angles became nearly random. In Fig. 2(g), we calculate the amplitudes of each band,

$$\Delta B_i = \sqrt{\int_{f_{lc,i}}^{f_{uc,i}} P_B(f) df}, \quad (1)$$

with the upper frequency cutoff $f_{uc,i}$ and the lower frequency cutoff $f_{lc,i}$ of the i th band, and then use the built-in function “MC_CORRELATE” in the Interactive Data Language software to evaluate the multiple correlation coefficient MC of $A_3 = \log_{10}(\Delta B_3)$ on $A_1 = \log_{10}(\Delta B_1)$ and $A_2 = \log_{10}(\Delta B_2)$. Specifically, let $A_3^* = aA_1 + bA_2$ be the best approximation of A_3 , and the usual correlation coefficient between A_3 and A_3^* is defined as the multiple correlation coefficient of A_3 on A_1 and A_2 . The obtained multiple correlation coefficient in this event is 0.6. Particularly after 19:45:03 UT, there was a one-to-one correlation between the fluctuations in the band 2 power and in the band 3 power. These observations raise the possibility of generation of the low-frequency hiss-like whistler waves (band 3) through the three-wave resonances with the two original normal chorus bands (bands 1 and 2).

In this case, the three-wave resonance conditions should be expressed as⁴⁷

$$f_3 = \Delta f \equiv f_1 - f_2, \quad (2)$$

$$\mathbf{k}_3 = \Delta \mathbf{k} \equiv \mathbf{k}_1 - \mathbf{k}_2, \quad (3)$$

where f and \mathbf{k} represent the wave frequencies and wave vectors, and their superscripts denote the numbers of the bands. In Fig. 3, we examine the resonance conditions for the three chorus bands. In order to see a clear view of the parameters of the chorus waves, Fig. 3 shows them in a shorter time range (2 s) than Fig. 2. The frequencies and wave normal angles are power-weighted values in each band. The power-weighted value is defined as

$$\rho_i^* = \frac{\sum_{f_{lc,i}}^{f_{uc,i}} P_B(f) \rho(f)}{\sum_{f_{lc,i}}^{f_{uc,i}} P_B(f)}, \quad (4)$$

where ρ_i^* is the power-weighted physical quantity of the i th band and $\rho(f)$ is a frequency dependent physical quantity. We have attempted to calculate wave vectors using full electric and magnetic field data. Considering the antenna sheath impedance,⁴⁸ we have used the relation $\mathbf{E} \cdot \mathbf{B} = 0$ to correct the electric component along the spin axis. However, we find that the obtained wave vectors exhibit large

fluctuations. This technique to calculate the wave vectors seems to not be reliable in this event, possibly because of the low coherency of waves. To allow further analysis, we obtain the wave vector $\mathbf{k} = k_{\parallel} \mathbf{e}_{\parallel} + k_{\perp} \mathbf{e}_{\perp}$ from the cold plasma dispersion relation,^{36,49}

$$\frac{k^2 c^2}{\omega_{pe}^2} = \frac{\omega^2}{\omega_{pe}^2} + \frac{\omega}{\omega_{ce} \cos \theta - \omega}, \quad (5)$$

with the inputs of wave angular frequency $\omega = 2\pi f^*$, wave normal angle θ^* , electron angular gyrofrequency $\omega_{ce} = 2\pi f_{ce}$, and the plasma frequency $\omega_{pe} = \sqrt{\frac{N_e e^2}{\epsilon_0 m_e}}$.

Clearly, the power-weighted frequencies of all three bands are roughly constant. The frequency of band 3 inferred from the resonance condition, $\Delta f \equiv f_1 - f_2$ [black dot line in Fig. 3(a)], well coincides with the power-weighted frequency f_3^* [black solid line in Fig. 3(a)], indicating that the frequencies of the three bands obey the resonance condition. Bands 1 and 2 have comparable values of θ^* and ψ^* . Probably because of the smoothing effect during the power weighted process over a broad frequency range, θ^* and ψ^* of band 1 exhibit weaker fluctuations than those of band 2. For the waves considered here, the magnitude of k_{\parallel} is basically dominated by f^* and weakly depends on θ^* . Hence, the parallel wave numbers k_{\parallel} fluctuate much more gently than the wave normal angles θ^* . As one can see, Δk_{\parallel} always lies within an acceptable error range of $k_{3\parallel}$, indicating the satisfaction of the resonance condition of the parallel wave number. Occasionally, the differences between Δk_{\parallel} and $k_{3\parallel}$ can exceed 50%, which corresponds to the spikes in $k_{1\parallel}$ and $k_{2\parallel}$ caused by the extreme values of θ_1^* and θ_2^* . In Fig. 3(e), the magnitudes of Δk_{\perp} and $k_{3\perp}$ are comparable to each other, but their correlation is not clear. There may be two reasons for the mismatch of k_{\perp} : (1) in contrast to k_{\parallel} , k_{\perp} can be highly affected by θ in the dispersion relation. The inaccuracies in the measurement of θ may cause significant errors of k_{\perp} and then the deviation between Δk_{\perp} and $k_{3\perp}$. (2) The estimated azimuthal angles ψ of \mathbf{k} vary rapidly over a wide range (larger than 180°), and consequently, the azimuthal angle difference between \mathbf{k}_1 and \mathbf{k}_2 is also not accurate enough to determine a reliable Δk_{\perp} . As usually done in previous studies,^{36,38} we give a possible range of Δk_{\perp} . Obviously, $k_{1\perp}$ and $k_{2\perp}$ will compose the minimum and maximum Δk_{\perp} when $\Delta\psi$ equals 0 and π , respectively. As shown in Fig. 3(f), most of the time, $k_{3\perp}$ is in the possible range. All these analyses tend to support that the low-frequency hiss-like whistler-mode waves were produced by the nonlinear coupling of the two normal chorus bands with higher frequencies.

In order to support the generality of the proposed mechanism, another event observed by Probe B on 30 September 2012 is shown in Fig. 4. In this event, there were also substorms (AE maximum of 1000 nT) but no storm (SYM-H > -30 nT). For brevity, we only show the burst-mode power spectral densities, amplitudes, and propagation characteristics of the waves. In this event, there were also normal chorus waves (bands 0–2) around $0.5 f_{ce}$, and a low-frequency whistler wave (band 3) extended down to ~ 200 Hz ($0.037 f_{ce}$). The multiple correlation coefficient of band 3 on bands 1 and 2 reaches 0.85, once again implying the action of the nonlinear three-wave interaction. Analogous to the situation in the previous event (Fig. 3), the resonance conditions for frequency f^* are well satisfied, Δk_{\parallel} is in the error range of $k_{3\parallel}$ most of the time, and $k_{3\perp}$ is almost always confined in the possible range of Δk_{\perp} . It should be noted that band 2 comprised some falling tones, different from the situation in the previous event (Fig. 2).

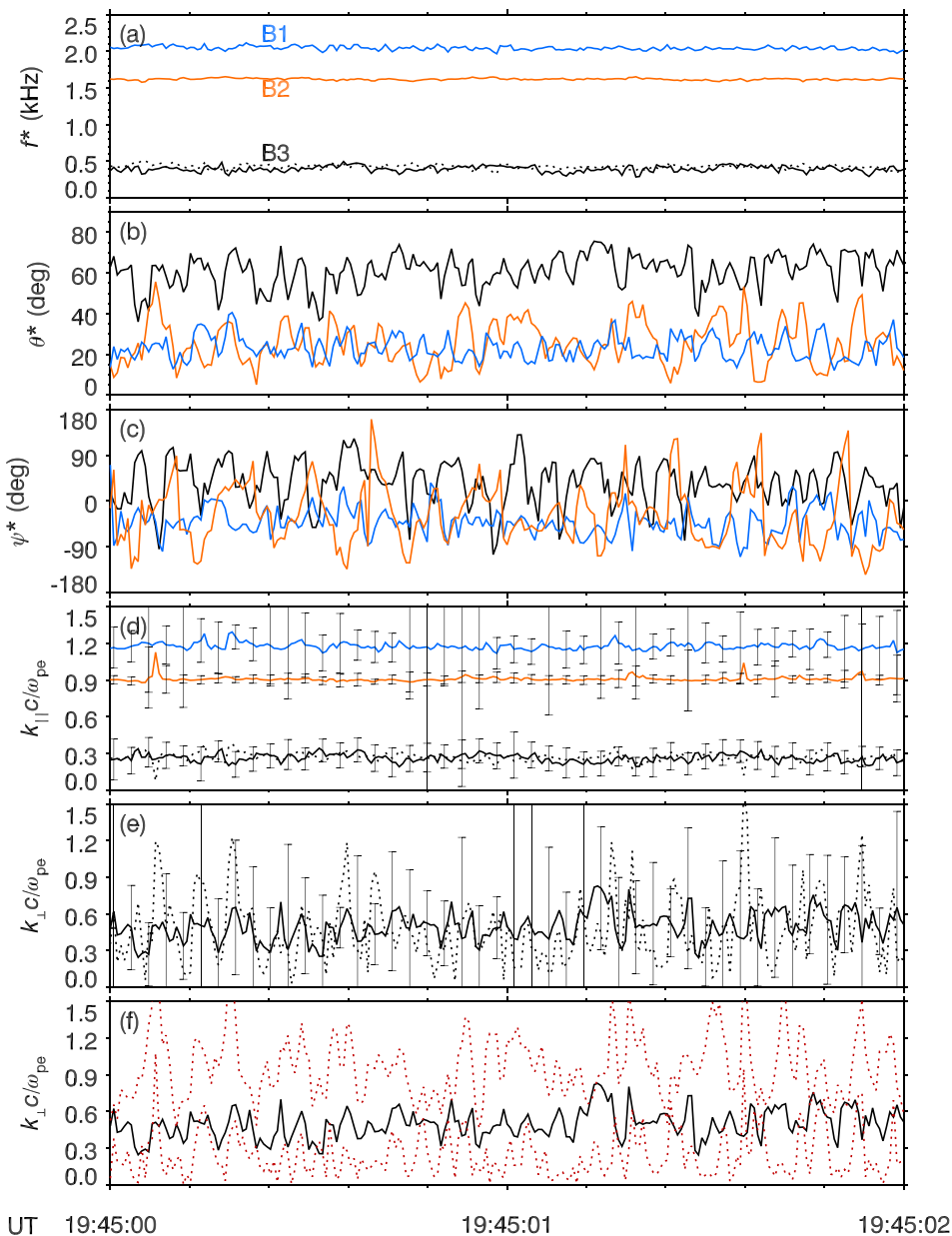


FIG. 3. Examination of three-wave resonance conditions among the whistler bands: power-weighted (a) frequencies f^* , (b) normal angles θ^* , (c) azimuthal angles ψ^* , normalized (d) parallel wave numbers k_{\parallel} , and [(e) and (f)] perpendicular wave numbers k_{\perp} . In these figures, the blue, orange, and black solid lines represent the corresponding properties of bands 1, 2, and 3, respectively, and the black dot lines represent the corresponding properties' differences between bands 1 and 2 (e.g., $\Delta f \equiv f_1 - f_2$, $\Delta k \equiv k_1 - k_2$). In Figs. 3(e) and 3(f), we only show the k_{\perp} of band 3. The two red dot lines in Fig. 3(f) are calculated Δk_{\perp} with two assumed azimuthal angle differences between bands 1 and 2, $\Delta\psi = 0$, and $\Delta\psi = \pi$. The error bars in Figs. 3(d) and 3(e) are the standard deviations of k_{\parallel} and k_{\perp} calculated for waves throughout each band.

Because the hiss-like band 1 had a much broader frequency range than band 2, their difference-frequency interaction still produced a hiss-like band.

IV. SUMMARY

Whistler-mode waves are one of the most important electromagnetic waves outside the plasmasphere. The wave frequency distribution characteristics will highly affect the direction and efficiency of energy transfer between the waves and particles. Recently, low-frequency whistler-mode chorus waves below $0.1 f_{ce}$ have gained considerable attention. In this paper, we describe a new type of low-frequency hiss-like whistler-mode wave around or below $0.1 f_{ce}$. For the two events, a

low-frequency whistler band appeared together with other normal chorus bands, and the multiple correlation coefficients of the low-frequency whistler band on another two chorus bands are 0.6 and 0.85. The comparison of the frequencies and wave numbers of these waves clearly shows that the three-wave resonance conditions were basically satisfied. These analyses support that the low-frequency hiss-like whistler-mode waves were produced by the nonlinear coupling of the two normal chorus bands with higher frequencies. This mechanism serves as an additional energy transfer process for the whistler-mode waves after their generation by the wave-particle interactions.

Our present study only reports two typical events of the low-frequency whistler waves generated by the three-wave interactions.

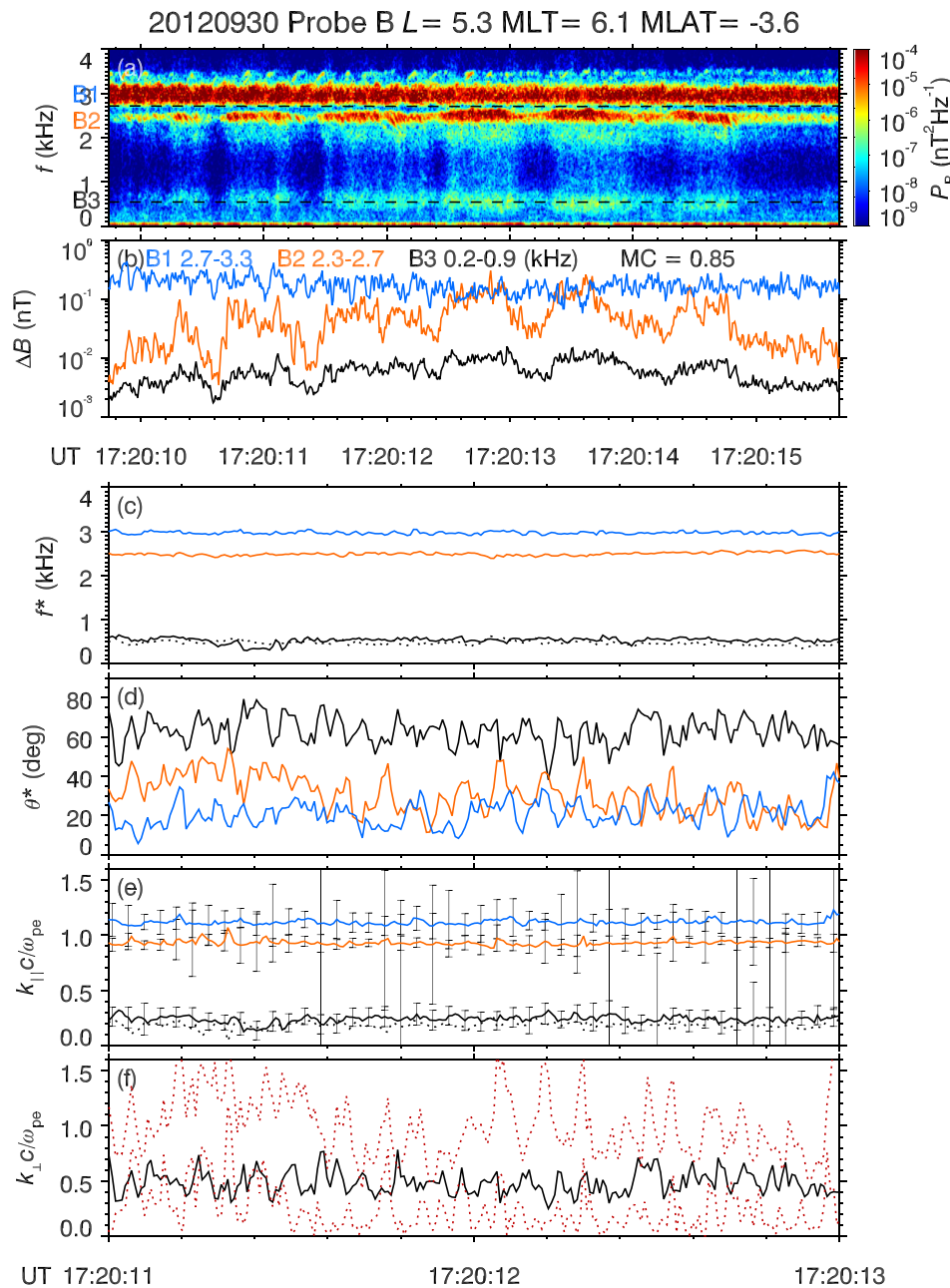


FIG. 4. Another burst-mode event of low-frequency whistler excited by the three-wave interaction observed by Probe B on 30 September 2012. (a) Magnetic power spectra P_B , (b) wave amplitudes ΔB , power-weighted (c) frequencies f^* , (d) normal angles θ^* , normalized (e) parallel wave numbers k_{\parallel} , and (f) perpendicular wave numbers k_{\perp} . The dashed lines in Fig. 4(a) represent 0.1 and 0.5 f_{ce} . The locations and frequency ranges of “B1, B2, and B3” are labeled in Figs. 4(a) and 4(b). In Figs. 4(b)–4(f), these solid and dot lines represent the same meanings as those in Fig. 3.

Compared with the normal chorus waves, the newly generated whistler waves have much lower frequencies and much larger wave normal angles. As shown in previous quasilinear calculations,^{15,50,51} the decrease in the wave frequency favors the pitch-angle scattering of high energy electrons, and the increase in the wave normal angles can enhance the pitch-angle scattering of energetic electrons with the contribution of the high-order cyclotron resonances. In the future, both statistical and numerical studies are required to determine the spatio-temporal distribution of the reported low-frequency whistler waves and evaluate their effect on the magnetospheric electrons.

ACKNOWLEDGMENTS

We acknowledge Van Allen Probes teams for the use of data. Data are available at the websites: <http://emfisis.physics.uiowa.edu/Flight/> for EMFISIS and http://www.rbsp-ect.lanl.gov/data_pub/ for ECT. This work was supported by the National Natural Science Foundation of China under Grant Nos. 41804171, 41731067, and 41822404, the Shenzhen Technology Project (Grant Nos. JCYJ20170307150645407, JCYJ20180306171748011, and ZDSYS201707280904031) and the China Postdoctoral Science Foundation 2019M661263.

REFERENCES

- ¹C. F. Kennel and H. E. Petschek, *J. Geophys. Res.* **71**(1), 1–28, <https://doi.org/10.1029/JZ071i001p00001> (1966).
- ²R. A. Helliwell, *J. Geophys. Res.* **72**, 4773, <https://doi.org/10.1029/JZ072i19p04773> (1967).
- ³N. P. Meredith, R. B. Horne, R. M. Thorne, and R. R. Anderson, *J. Geophys. Res.* **114**, A07218, <https://doi.org/10.1029/2009JA014230> (2009).
- ⁴F. Xiao, C. Yang, Z. Su, Q. Zhou, Z. He, Y. He, D. Baker, H. Spence, H. Funsten, and J. Blake, *Nat. Commun.* **6**, 8590 (2015).
- ⁵H. S. Fu, J. B. Cao, B. Yang, and H. Y. Lu, *J. Geophys. Res.* **116**, A10210, <https://doi.org/10.1029/2011JA016672> (2011).
- ⁶D. Summers, R. M. Thorne, and F. Xiao, *J. Geophys. Res.* **103**, 20487, <https://doi.org/10.1029/98JA01740> (1998).
- ⁷R. M. Thorne, W. Li, B. Ni, Q. Ma, J. Bortnik, L. Chen, D. N. Baker, H. E. Spence, G. D. Reeves, M. G. Henderson, C. A. Kletzing, W. S. Kurth, G. B. Hospodarsky, J. B. Blake, J. F. Fennell, S. G. Claudepierre, and S. G. Kanekal, *Nature* **504**, 411 (2013).
- ⁸F. Xiao, Z. Su, H. Zheng, and S. Wang, *J. Geophys. Res.* **114**, A03201, <https://doi.org/10.1029/2008JA013580> (2009).
- ⁹F. Xiao, Z. Su, H. Zheng, and S. Wang, *J. Geophys. Res.* **115**, A05216, <https://doi.org/10.1029/2010JA015374> (2010).
- ¹⁰Z. Su, F. Xiao, H. Zheng, Z. He, H. Zhu, M. Zhang, C. Shen, Y. Wang, S. Wang, C. A. Kletzing, W. S. Kurth, G. B. Hospodarsky, H. E. Spence, G. D. Reeves, H. O. Funsten, J. B. Blake, and D. N. Baker, *Geophys. Res. Lett.* **41**, 229, <https://doi.org/10.1002/2013GL058912> (2014).
- ¹¹H. S. Fu, J. B. Cao, Q.-G. Zong, H. Y. Lu, S. Y. Huang, X. H. Wei, and Y. D. Ma, *J. Atmos. Sol.-Terr. Phys.* **80**, 37 (2012).
- ¹²B. Ni, R. M. Thorne, Y. Y. Shprits, and J. Bortnik, *Geophys. Res. Lett.* **35**, L11106, <https://doi.org/10.1029/2008GL034032> (2008).
- ¹³Z. Su, H. Zheng, and S. Wang, *J. Geophys. Res.* **115**, A05219, <https://doi.org/10.1029/2010JA015903> (2010).
- ¹⁴H. Zhu, Z. Su, F. Xiao, H. Zheng, Y. Wang, C. Shen, T. Xian, S. Wang, C. Kletzing, W. S. Kurth *et al.*, *Geophys. Res. Lett.* **42**, 1012, <https://doi.org/10.1002/2014GL062964> (2015).
- ¹⁵Z. Gao, Z. Su, H. Zhu, F. Xiao, H. Zheng, Y. Wang, C. Shen, and S. Wang, *Geophys. Res. Lett.* **43**, 967, <https://doi.org/10.1002/2016GL067687> (2016).
- ¹⁶B. T. Tsurutani and E. J. Smith, *J. Geophys. Res.* **79**, 118, <https://doi.org/10.1029/JA079i001p00118> (1974).
- ¹⁷O. Santolík, D. A. Gurnett, J. S. Pickett, M. Parrot, and N. Cornilleau-Wehrlein, *J. Geophys. Res.* **108**, 1278, <https://doi.org/10.1029/2002JA009791> (2003).
- ¹⁸W. J. Burtis and R. A. Helliwell, *Planet. Space Sci.* **24**, 1007 (1976).
- ¹⁹W. Li, R. M. Thorne, J. Bortnik, X. Tao, and V. Angelopoulos, *Geophys. Res. Lett.* **39**, L18106, <https://doi.org/10.1029/2012GL053206> (2012).
- ²⁰H. S. Fu, J. B. Cao, C. M. Cully, Y. V. Khotyaintsev, A. Vaivads, V. Angelopoulos, Q.-G. Zong, O. Santolík, E. Macúšová, M. André, W. L. Liu, H. Y. Lu, M. Zhou, S. Y. Huang, and Z. Zhima, *J. Geophys. Res.: Space Phys.* **119**, 9089, <https://doi.org/10.1002/2014JA020204> (2014).
- ²¹H. S. Fu, J. B. Cao, F. S. Mozer, H. Y. Lu, and B. Yang, *J. Geophys. Res.* **117**, A01203, <https://doi.org/10.1029/2011JA016913> (2012).
- ²²Z. Su, H. Zhu, F. Xiao, H. Zheng, Y. Wang, Z. He, C. Shen, C. Wang, R. Liu, M. Zhang, S. Wang, C. A. Kletzing, W. S. Kurth, G. B. Hospodarsky, H. E. Spence, G. D. Reeves, H. O. Funsten, J. B. Blake, D. N. Baker, and J. R. Wygant, *J. Geophys. Res.* **119**, 4266, <https://doi.org/10.1002/2014JA019919> (2014).
- ²³F. Xiao, Q. Zhou, H. Zheng, and S. Wang, *J. Geophys. Res.* **111**, A08208, <https://doi.org/10.1029/2006JA011612> (2006).
- ²⁴D. Nunn, Y. Omura, H. Matsumoto, I. Nagano, and S. Yagitani, *J. Geophys. Res.* **102**, 27083, <https://doi.org/10.1029/97JA02518> (1997).
- ²⁵Y. Omura, Y. Katoh, and D. Summers, *J. Geophys. Res.* **113**, A04223, <https://doi.org/10.1029/2007JA012622> (2008).
- ²⁶H. S. Fu, J. B. Cao, Z. Zhima, Y. V. Khotyaintsev, V. Angelopoulos, O. Santolík, Y. Omura, U. Taubenschuss, L. Chen, and S. Y. Huang, *Geophys. Res. Lett.* **41**, 7419, <https://doi.org/10.1002/2014GL061867> (2014).
- ²⁷R. M. Thorne, E. J. Smith, R. K. Burton, and R. E. Holzer, *J. Geophys. Res.* **78**, 1581, <https://doi.org/10.1029/JA078i010p01581> (1973).
- ²⁸Z. Gao, Z. Su, F. Xiao, H. Zheng, Y. Wang, S. Wang, H. E. Spence, G. D. Reeves, D. N. Baker, J. B. Blake, and H. O. Funsten, *Earth Planet. Phys.* **2**, 1 (2018).
- ²⁹J. Bortnik, R. M. Thorne, and N. P. Meredith, *Nature* **452**, 62 (2008).
- ³⁰N. Liu, Z. Su, Z. Gao, H. Zheng, Y. Wang, and S. Wang, *Geophys. Res. Lett.* **46**, 1900, <https://doi.org/10.1029/2018GL081500> (2019).
- ³¹C. Cattell, A. Breneman, S. Thaller, J. Wygant, C. Kletzing, and W. Kurth, *Geophys. Res. Lett.* **42**, 7273–7281, <https://doi.org/10.1002/2015GL065565> (2015).
- ³²F. Xiao, S. Liu, X. Tao, Z. Su, Q. Zhou, C. Yang, Z. He, Y. He, Z. Gao, D. N. Baker, H. E. Spence, G. D. Reeves, H. O. Funsten, and J. B. Blake, *J. Geophys. Res.: Space Phys.* **122**, 3201, <https://doi.org/10.1002/2016JA023561> (2017).
- ³³X. Yu, Z. Yuan, S. Huang, F. Yao, Z. Qiao, J. R. Wygant, and H. O. Funsten, *Earth Planet. Phys.* **3**(1), 1–7 (2019).
- ³⁴Z. Su, N. Liu, H. Zheng, Y. Wang, and S. Wang, *Geophys. Res. Lett.* **45**, 565, <https://doi.org/10.1002/2017GL076754> (2018).
- ³⁵Z. Su, N. Liu, H. Zheng, Y. Wang, and S. Wang, *Geophys. Res. Lett.* **45**, 10, <https://doi.org/10.1029/2018GL079927> (2018).
- ³⁶X. Gao, Q. Lu, and S. Wang, *Geophys. Res. Lett.* **44**, 5269, <https://doi.org/10.1002/2017GL073829> (2017).
- ³⁷X. Fu, S. P. Gary, G. D. Reeves, D. Winske, and J. R. Woodroffe, *Geophys. Res. Lett.* **44**, 9532, <https://doi.org/10.1002/2017GL074411> (2017).
- ³⁸S. Teng, J. Zhao, X. Tao, S. Wang, and G. Reeves, *Geophys. Res. Lett.* **45**, 6343, <https://doi.org/10.1029/2018GL078765> (2018).
- ³⁹N. Liu, Z. Su, H. Zheng, Y. Wang, and S. Wang, *Geophys. Res. Lett.* **45**, 7985–7995, <https://doi.org/10.1029/2018GL079232> (2018).
- ⁴⁰B. H. Mauk, N. J. Fox, S. G. Kanekal, R. L. Kessel, D. G. Sibeck, and A. Ukhorskiy, *Space Sci. Rev.* **179**, 3 (2013).
- ⁴¹H. O. Funsten, R. M. Skoug, A. A. MacDonald, J. R. Baldonado, R. W. Harper, K. C. Henderson, K. H. Kihara, J. E. Lake, B. A. Larsen, A. D. Puckett, V. J. Vigil, R. H. Friedel, M. G. Henderson, J. T. Niehof, G. D. Reeves, M. F. Thomsen, J. J. Hanley, D. E. George, J.-M. Jahn, S. Cortinas, A. De Los Santos, G. Dunn, E. Edlund, M. Ferris, M. Freeman, M. Maple, C. Nunez, T. Taylor, W. Toczynski, C. Urdiales, H. E. Spence, J. A. Cravens, L. L. Suther, and J. Chen, *Space Sci. Rev.* **179**, 423 (2013).
- ⁴²J. B. Blake, P. A. Carranza, S. G. Claudepierre, J. H. Clemons, W. R. Crain, Y. Dotan, J. F. Fennell, F. H. Fuentes, R. M. Galvan, J. S. George, M. G. Henderson, M. Lalic, A. Y. Lin, M. D. Looper, D. J. Mabry, J. E. Mazur, B. McCarthy, C. Q. Nguyen, T. P. O'Brien, M. A. Perez, M. T. Redding, J. L. Roeder, D. J. Salvaggio, G. A. Sorensen, H. E. Spence, S. Yi, and M. P. Zakrzewski, *Space Sci. Rev.* **179**, 383 (2013).
- ⁴³H. E. Spence, G. D. Reeves, D. N. Baker, J. B. Blake, M. Bolton, S. Bourdarie, A. H. Chan, S. G. Claudepierre, J. H. Clemons, J. P. Cravens, S. R. Elkington, J. F. Fennell, R. H. W. Friedel, H. O. Funsten, J. Goldstein, J. C. Green, A. Guthrie, M. G. Henderson, R. B. Horne, M. K. Hudson, J.-M. Jahn, V. K. Jordanova, S. G. Kanekal, B. W. Klatt, B. A. Larsen, X. Li, E. A. MacDonald, I. R. Mann, J. Niehof, T. P. O'Brien, T. G. Onsager, D. Salvaggio, R. M. Skoug, S. S. Smith, L. L. Suther, M. F. Thomsen, and R. M. Thorne, *Space Sci. Rev.* **179**, 311 (2013).
- ⁴⁴C. A. Kletzing, W. S. Kurth, M. Acuna, R. J. MacDowall, R. B. Torbert, T. Averkamp, D. Bodet, S. R. Bounds, M. Chutter, J. Connerney, D. Crawford, J. S. Dolan, R. Dvorsky, G. B. Hospodarsky, J. Howard, V. Jordanova, S. G. Kanekal, D. Kirchner, B. Mokrzycki, G. Needell, J. Odom, D. Mark, R. Pfaff, J. R. Phillips, C. W. Piker, S. L. Remington, D. Rowland, O. Santolik, R. Schmurr, D. Sheppard, C. W. Smith, R. M. Thorne, and J. Tyler, *Space Sci. Rev.* **179**, 127 (2013).
- ⁴⁵O. Santolík, M. Parrot, and F. Lefevre, *Radio Sci.* **38**, 1010, <https://doi.org/10.1029/2000RS002523> (2003).
- ⁴⁶N. A. Tsyganenko and M. I. Sitnov, *J. Geophys. Res.* **110**, A03208, <https://doi.org/10.1029/2004JA010798> (2005).
- ⁴⁷T. Boyd, T. Boyd, and J. Sandercock, *The Physics of Plasmas* (Cambridge University Press, 2003), pp. 390–392.
- ⁴⁸D. P. Hartley, C. A. Kletzing, W. S. Kurth, S. R. Bounds, T. F. Averkamp, G. B. Hospodarsky, J. R. Wygant, J. W. Bonnell, O. Santolík, and C. E. J. Watt, *J. Geophys. Res.: Space Phys.* **121**, 4590, <https://doi.org/10.1002/2016JA022501> (2016).
- ⁴⁹D. Mourenas, A. V. Artemyev, O. V. Agapitov, V. Krasnoselskikh, and F. S. Mozer, *J. Geophys. Res.: Space Phys.* **120**, 3665, <https://doi.org/10.1002/2015JA021135> (2015).
- ⁵⁰D. Mourenas, A. Artemyev, O. Agapitov, and V. Krasnoselskikh, *J. Geophys. Res.* **117**, A10212, <https://doi.org/10.1029/2011JA016985> (2012).
- ⁵¹A. Artemyev, O. Agapitov, H. Breuillard, V. Krasnoselskikh, and G. Rolland, *Geophys. Res. Lett.* **39**, L08105, <https://doi.org/10.1029/2012GL051393> (2012).